Available online at www.sciencedirect.com
ScienceDirect
C. R. Mecanique 337 (2009) 395–405
COMPTES RENDUS MECANIQUE

Combustion for aerospace propulsion

Dynamics of premixed confined swirling flames

P. Palies [a,*], D. Durox [a], T. Schuller [a], P. Morenton [b], S. Candel [a,c]

[a] *Laboratoire EM2C CNRS, École centrale Paris, grande voie des vignes, 92295 Châtenay Malabry, France*
[b] *Laboratoire génie industriel, École centrale Paris, grande voie des vignes, 92295 Châtenay Malabry, France*
[c] *Institut Universitaire de France*

Available online 21 July 2009

Abstract

Considerable effort is currently being extended to examine the fundamental mechanisms of combustion instabilities and develop methods allowing predictions of these phenomena. One central aspect of this problem is the dynamical response of the flame to incoming perturbations. This question is examined in the present article, which specifically considers the response of premixed swirling flames to perturbations imposed on the upstream side of the flame in the feeding manifold. The flame response is characterized by measuring the unsteady heat release induced by imposed velocity perturbations. A flame describing function is defined by taking the ratio of the relative heat release rate fluctuation to the relative velocity fluctuation. This quantity is determined for a range of frequencies and for different levels of incoming velocity perturbations. The flame dynamics is also documented by calculating conditional phase averages of the light emission from the flame and taking the Abel transform of these average images to obtain the flame geometry at various instants during the cycle of oscillation. These data can be useful to the determination of possible regimes of instability. ***To cite this article: P. Palies et al., C. R. Mecanique 337 (2009).***

Résumé

Dynamique de flammes prémélangées, confinées et swirlées. Un effort de recherche important est actuellement effectué pour comprendre les mćanismes fondamentaux qui contrôlent les instabilitś de combustion et pour développer des méthodes permettant de prévoir ces phénomènes. Un aspect central de ce probléme est la réponse dynamique des flammes à des perturbations amont. Cette question est abordé dans cet article qui considère spécifiquement la réponse de flammes prémélangées et swirlées à des perturbations de vitesse imposées en amont du brûleur. Cette réponse de flamme est caractérisée par la mesure du taux de dégagement de chaleur de la flamme induit par les perturbations de vitesses. Une fonction de transfert généralisée (FDF pour "*Flame Describing Function*") est alors définie en prenant le rapport du dégagement de chaleur relatif et de la fluctuation de vitesse relative. Cette quantité est déterminé pour une gamme de fréquence et pour plusieurs amplitudes de la fluctuation de vitesse. La dynamique de flamme est aussi étudiée à l'aide des images d'émission moyennes conditionnées par la phase et traitées par transformé d'Abel pour obtenir la géométrie de la flamme à différents instants du cycle d'excitation. L'ensemble de ces résultats peuvent être utiles à la détermination des régimes d'instabilités possibles. ***Pour citer cet article : P. Palies et al., C. R. Mecanique 337 (2009).***

Keywords: Combustion; Swirl; Flame describing function; Acoustic coupling; Confinement

Mots-clés : Combustion ; Swirl ; Fonction de transfert généralisés ; Couplage acoustique ; Confinement

* Corresponding author.
E-mail address: paul.palies@em2c.ecp.fr (P. Palies).

1631-0721/$ – see front matter
doi:10.1016/j.crme.2009.06.001

1. Introduction

Current objectives in terms of pollutant emission reduction induce difficult design and operational challenges to the gas turbine industry. One objective is to diminish NO_x emission while keeping other pollutants like CO at a low level. This is accomplished by making use of advanced combustion concepts in which reactants are injected in premixed form at a relatively lean equivalence ratio. This mode of operation is quite attractive but raises combustion dynamics problems. Lean premixed flames are sensitive to external perturbations [1,2] and premixed operation near the lean blowout can lead to oscillations, flashback or extinction. The standard method used to stabilize flames in current lean-premixed combustors is based on swirling injection. Combustion is established around a hot gas kernel formed by the swirling flow. The lower pressure region created in the central region by swirl generates an internal recirculation zone of burnt gases anchoring the flame. This region designated as the inner recirculation zone (IRZ) is associated with the vortex breakdown process which takes place in swirling flows [3,4]. The intensity and shape of this IRZ mainly depends on the rate of rotation induced by swirl and on the combustor geometry. The rate of rotation is characterized by the swirl number [5] defined as the ratio of the tangential to axial momentum:

$$S = \frac{\int_0^R \rho v_\theta v_z 2\pi r^2 \,\mathrm{d}r}{R \int_0^R \rho v_z^2 2\pi r \,\mathrm{d}r} \tag{1}$$

where ρ is the density of the fluid, v_θ the azimuthal velocity, v_z the axial velocity and R the characteristic outer radius. In this expression, the pressure term in the axial momentum flux is neglected. It is known that the inner recirculation zone is well defined for swirl numbers of at least 0.6. This value, or slightly higher, is found in typical industrial combustors. Another stabilization mechanism is linked to the outer recirculation zone (ORZ) [3,4,6] which is formed by recirculation of gases trapped between the flame and the combustor walls and backplane.

To control and avoid combustion instabilities in modern combustion chambers equipped with swirl injectors, it is necessary to study the sensitivity and dynamical response of swirling flames to incoming disturbances. Perturbations of various types need to be considered. One important class is formed by velocity fluctuations which accompany pressure oscillations [7,8]. Another type of perturbation consists in equivalence ratio disturbances [9], which can be created by the differential response of fuel and air injectors to pressure waves generated by thermo-acoustic instabilities. Oscillations in the combustor are themselves induced by a coupling between the unsteady fluctuations of heat release rate and the unsteady pressure in the chamber [1,10,11]. A number of studies focus on combustion instabilities of systems equipped with swirl injectors [12–17]. It is however of fundamental importance to examine the flame dynamics by investigating the response to well controlled externally imposed perturbations. This aspect is already covered by some articles which consider the dynamics of swirling flames experimentally [7,8,18,19] or numerically through RANS [20] or through the more advanced LES approach [21–24]. Simulations can be used to optimize the steady state performance of swirling injectors but it is still important to validate unsteady numerical calculations in well controlled configurations. It is also essential to understand dynamical processes and take into account the nonlinearities associated with the flame and combustor responses. Experimental work indicates that the IRZ is quite sensitive and that its intensity and location can be influenced by incoming perturbations [6–8]. Previous studies also indicate that swirl flame dynamics is linked to vortex roll-up processes taking place in the injection region and involving the flame tip [7,8,17,19]. This class of phenomena has been studied for laminar and turbulent "V" flames respectively in [25,26]. Vortices are shed from the injector nozzle lip in response to the flow modulations rolling-up the flame edge. One direct effect of the swirl number is to change the flame spreading angle modifying the distance between the nozzle and the flame front. In an unconfined flame study [19] it is concluded that at large swirl numbers (0.79), the flame is more susceptible to instabilities, and that its response can amplify the perturbation. However, in the unconfined configuration, ambient air is entrained and it is difficult to extend the results obtained to more practical confined cases where the ORZ is also present. Others authors [6] evoke the nonlinear behavior of swirling flames submitted to various levels of mass flow fluctuations. It is shown that the unsteady shape of the flame is a strong function of the mass flow rate fluctuation level. It is then not easy to determine a time delay between flow rate fluctuations and resulting perturbations in heat release rate. Experiments indicate that the flame response saturates when the mass flow rate fluctuation is augmented. With the exception of Refs. [6] and [8] there are few papers dealing with the effect of flow modulations on the dynamics of confined swirling flames while the corresponding data are needed to predict thermo-acoustic instabilities in combustion chambers.

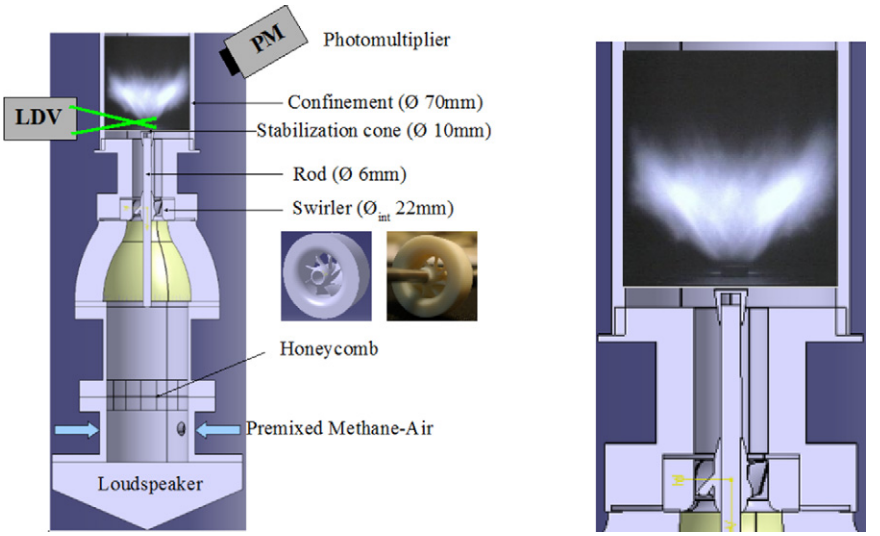

Fig. 1. Left: schematic view of the burner and diagnostics used for measurements. Right: close-up view of the upper part of the burner.

The present article tries to fill this need. It first concentrates on the burner system design and on the definition of the axial swirler geometry. This is based on an iterative optimization loop. Axial and azimuthal velocity profiles obtained by laser Doppler anemometry are used to determine the effective swirl number (Section 2). The burner is then used to characterize the flame dynamics induced by axial velocity fluctuations. Transfer functions are measured for different levels of incoming perturbations. This family of transfer functions forms a "flame describing function" (FDF) which depends on frequency and amplitude of the incoming disturbance (Section 3). Two sets of results corresponding to different mass flow rates are reported. An analysis of phase conditioned images of the flame region is carried out in the last section. A set of images is obtained by making use of phase averaging to extract the oscillation of the flame during a cycle. The average emission images are Abel transformed to obtain a slice through the flame and determine the evolution of the reaction layer as a function of time (Section 3).

2. Design, optimization and steady flow configuration

The burner sketched in Fig. 1 comprises a standard body including a driver unit, a settling chamber, a contraction ended by a constant diameter duct, a horizontal end piece and a cylindrical flame tube. An air/methane premixed flow is delivered to the premixing unit through two diametrically opposed apertures. The equivalence ratio is set equal to $\phi = 0.7$. The flow crosses a grid and a honeycomb in order to break the largest turbulent scales. The gas then traverses a convergent unit to reduce the boundary layer thickness, diminish the level of turbulence and generate a flat velocity profile at the swirler input. The rotation of the flow is induced by the swirler equipped with eight twisted vanes arranged periodically around a central rod (6 mm in diameter). This central rod is terminated with a small cone (10 mm in diameter at its base) which stabilizes the flame during the unsteady motion of the flow. In this way, flashback is minimized. The outer diameter of the injector is 22 mm. The tube confining the flame is made of quartz allowing optical visualization of the flame and transmitting its radiation in the near ultraviolet. Its diameter is 70 mm and its length 100 mm.

The geometry of the swirler was specified to obtain a predetermined value of the swirl number corresponding to a flow featuring an inner recirculation zone. Experimental profiles of axial and azimuthal velocities, presented in what follows, indicate that the swirl number obtained with this device and estimated from expression (1) is about 0.55. All results presented in this article correspond to this swirl number but another swirler is now being designed to obtain higher rates of rotation. To keep the turbulence intensity low the swirler blades use NACA four digits wing section profiles. The general objective was to make sure that the level of fluctuations was lower than the level of disturbances imposed by acoustic modulations. Detailed views of the swirler are given in Fig. 2. The result of the design process is a swirler comprising eight vanes periodically spaced with a stagger angle of 45°. The vane section is that of a NACA 8411 airfoil. The swirler has twisted vanes, so that the angle at the trailing edge evolves linearly from 30° at the hub

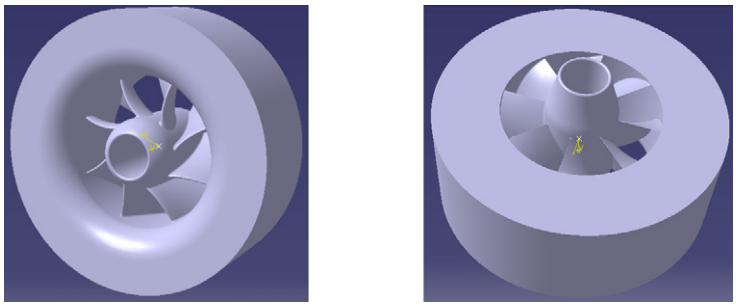

Fig. 2. View of the swirler. On the left, the upstream side of the swirler. On the right, the downstream side of the swirler.

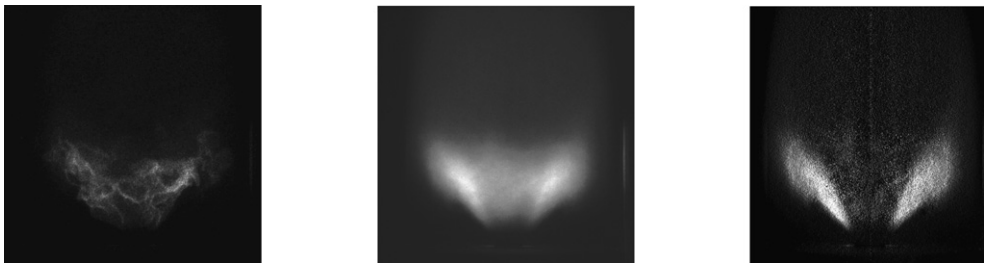

Fig. 3. From left to the right: (a) Instantaneous images of the flame, (b) Average of 100 instantaneous images, (c) Abel transform of the average image providing a two-dimensional slice through the flame. Operating point A: $\phi = 0.7$ and $U_b = 2.67\ \mathrm{m\,s^{-1}}$.

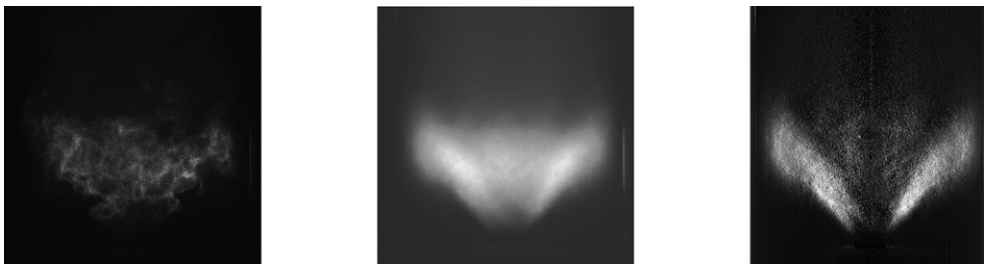

Fig. 4. From left to the right: (a) Instantaneous images of the flame, (b) Average of 100 instantaneous images, (c) Abel transform of the average image providing a two-dimensional slice through the flame. Operating point B: $\phi = 0.7$ and $U_b = 4.16\ \mathrm{m\,s^{-1}}$.

to a value of 58° at the vane tip. Twisting is employed in order to impose a rotation to the flow at all points along the vane. In the absence of twist there are regions near the vane tip in which the flow might not be deflected. The first version of the swirler was fabricated by fast prototyping of plastic material. The surface quality is moderately smooth but sufficient for the present purpose.

It is first interesting to examine two mean flow configurations for two selected operating points A and B corresponding respectively to mean flow velocities U_b of 2.67 $\mathrm{m\,s^{-1}}$ and 4.16 $\mathrm{m\,s^{-1}}$. The corresponding steady flame configurations are shown in Figs. 3 and 4. Flame B is longer than flame A, the size being related to the injection flow velocity. It is also found that the tip of flame B touches the quartz confinement tube while flame A is more compact and remains away from the lateral boundary. Figs. 3 and 4 display three images of the flame. The first corresponds to an instantaneous image of the flame region. This shows the highly wrinkled flame pattern formed by the system. The second image is an ensemble average of a hundred instantaneous images which highlights the steady flame pattern. The third image is obtained by taking the Abel transform of the average image. This yields a slice through the mean flame. The Abel transform is applicable if the average flame is effectively rotationally symmetric. The previous images indicate that the flame volume and flame size are larger for flame B. One also finds that the shapes of flames A and B are quite similar, except near the wall for flame B where the flame front bends slightly to follow the wall.

It is now instructive to consider the steady mean velocity profile at a close distance from the swirler (Fig. 5). These data are obtained with a laser Doppler velocimetry system. The measurement volume was located at 4 mm

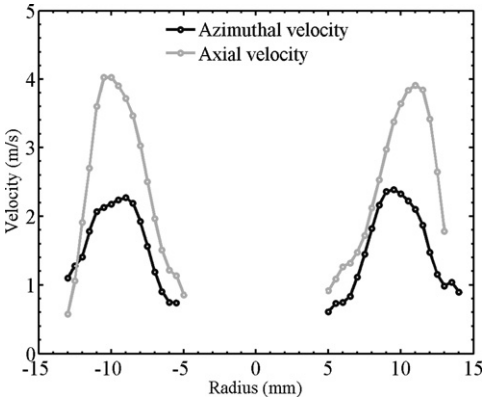

Fig. 5. Axial and azimuthal velocity profiles measured for operating point A corresponding to a bulk velocity $U_b = 2.67\ \mathrm{m\,s^{-1}}$ and $\phi = 0.7$.

downstream of the injector outlet. The flow was seeded with fine oil droplets of 2.5 μm in diameter generated by a perfume atomizer [27]. The maximum axial velocity is about twice the maximum azimuthal velocity. The swirl number can be deduced from the velocity profiles. For condition A the swirl number is close to 0.55. The same value is obtained for point B.

3. Flame describing functions

It is now interesting to examine the flame response to incident velocity perturbations. Various studies have already been carried out in laminar "V" flame geometries [25,28]. This has provided a set of data to determine the flame transfer function. The case of swirling flames is less well documented. Incomplete flame transfer functions are available for turbulent "V" flame configurations [14,26] and for an unconfined "V" flame [19]. A more complete study is presented in [6] although the swirl number is not really expressed and only assumed. Much of the work, devoted to flame dynamics, is motivated by the understanding of the nonlinear processes induced by large amplitude disturbances. It has been shown recently [29] that these issues can be addressed by making use of the flame describing function (FDF) defined by taking the ratio of the relative heat release rate fluctuation to the relative velocity fluctuation. This quantity is determined for a range of frequencies and for different levels of incoming velocity perturbations. The FDF may be defined by:

$$\mathcal{F}(\omega, U') = \frac{\dot{Q}'/\bar{\dot{Q}}}{U'/\bar{U}} \tag{2}$$

The heat release rate is usually obtained by recording the global emission signals of excited radicals like CH* or OH*. In the present study, the heat release rate is deduced from OH* emission and the axial velocity disturbance is measured with a LDV system. One can write this flame describing function as a function of the OH* chemiluminescence signal or the flame surface. Therefore:

$$\mathcal{F}(\omega, U') = \frac{\dot{Q}'/\bar{\dot{Q}}}{U'/\bar{U}} = \frac{I'_{\mathrm{OH}^*}/\bar{I}_{\mathrm{OH}^*}}{U'/\bar{U}} \sim \frac{\mathcal{A}'/\bar{\mathcal{A}}}{U'/\bar{U}} \tag{3}$$

The flame describing function can be expressed as a complex number in terms of a gain G and a phase difference φ. The flame transfer function is then expressed as:

$$\mathcal{F}(\omega, U') = G(\omega, U')e^{i\varphi(\omega, U')} \tag{4}$$

The gain reflects the level of response while the phase defines the time delay between velocity and emission signals. The FDF obtained for flame A (Fig. 6) pertains to a flow with a bulk velocity $U_b = 2.67\ \mathrm{m\,s^{-1}}$. It is determined in a frequency range extending from 0 to 400 Hz and corresponds to four velocity modulation levels U'/U_b: 0.3, 0.41, 0.51 and 0.72 where U' corresponds to the rms perturbation level determined at $z = 2.9$ mm from the injector outlet and at $r = 8$ mm from the axis. The gain approaches one in the low frequency limit. It decreases in a first range between

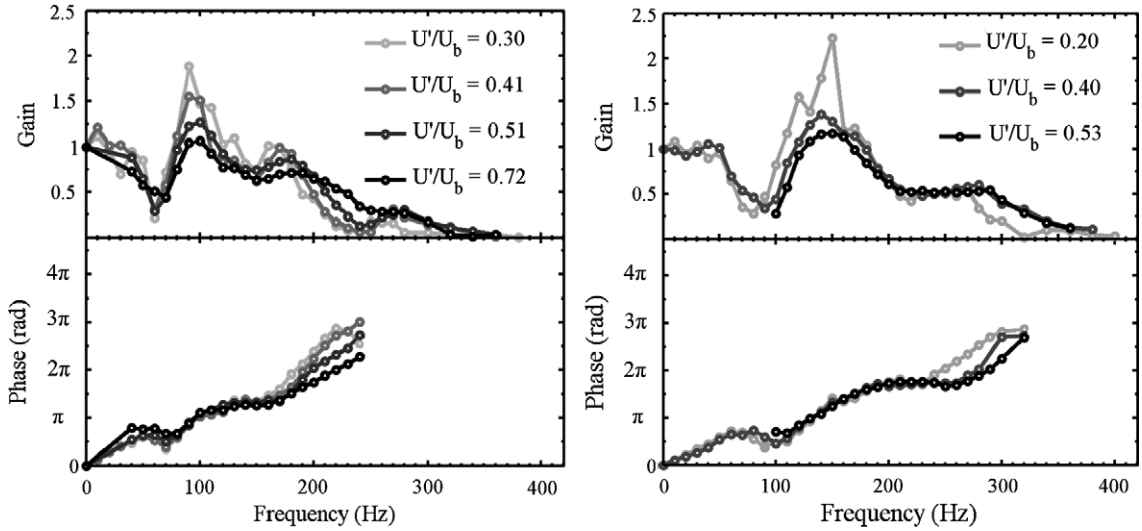

Fig. 6. Left: Flame describing function of flame A. Right: Flame describing function of flame B.

0 and 60 Hz to a value of less than 0.5. From 60 to 100 Hz, each curve features a peak. For all velocity disturbance levels, this peak is the maximum in the frequency range of interest. At 100 Hz, the flame response is highest. Beyond 100 Hz and up to 150 Hz, the gain drops again and reaches a value of 0.75 for most of the transfer function curves. From 150 to 180 Hz, the gain increases to reach a local maximum of about 1 (for the smallest modulation level) and 0.75 (for the highest modulation level). Beyond 180 Hz the gain decreases in all cases and drops to zero. The phase increases nearly continuously with frequency in the range from 0 to 250 Hz. Beyond 250 Hz, the phase is less smooth due to the low value of the gain in that frequency range. Under these conditions the phase estimates become unreliable. The phase signal can be used to determine a global delay of the dynamical interaction between the incoming velocity modulation and the resulting heat release rate perturbation. If the phase varies in an approximately linear way with respect to frequency, it is possible to write $\varphi = \omega\tau_{cv}$ where $\omega = 2\pi f$. This yields: $\varphi = 2\pi f \tau_{cv}$. This can be used to estimate the delay, which is in this case associated to a convective time: $\tau_{cv} = \varphi/2\pi f$. This convective delay which is approximately equal to 5 ms in the frequency range of interest corresponds to the time required by a disturbance to be convected to the flame and impinge on the flame edge. This can be seen by calculating this delay for the flame geometry under investigation: $\tau_d \simeq L/U_b$ where L is a characteristic length of the flame under unsteady operation and U_b is the bulk velocity. In this particular case, L equals 1.5 cm and U_b is 2.67 m s^{-1}. Then the associated delay is 5.6 ms which is close to the characteristic delay deduced from the transfer function phase. While the phase evolution is roughly linear, there are also ripples and a slight decrease around 70 Hz where the gain is small. The describing function shown in Fig. 6 was obtained for flame B corresponding to a larger flow velocity of 4.16 m s^{-1}. The frequency range of interest now extends from 0 to 400 Hz. Three velocity disturbance levels U'/U_b: 0.2, 0.4 and 0.53 are considered in this case. Data are lacking for the highest velocity disturbance level in the range 0–100 Hz because the flame flashes back into the burner when forced by the loudspeaker. From 0 to 60 Hz, the gain is constant and close to a value of one. From 60 to 100 Hz, the gain diminishes and reaches a low value of 0.3. From 100 to 150 Hz, the gain increases and reaches a local maximum for the three curves. From 150 to 200 Hz, the gain decreases and reaches a value of 0.6. This value remains constant in the frequency range 200–280 Hz. For frequencies exceeding 280 Hz and up to 400 Hz, the gain decreases finally dropping to zero. The general trend for the phase is quasi-linear from 0 to 400 Hz but there are undulations and the different curves composing the FDF do not quite collapse. To compare results obtained for the two flames, it is logical to replace the dimensional frequency by a reduced angular frequency ω^*, or by a Strouhal number. It is clearly interesting to consider this possibility. The definition of the reduced angular frequency can be based on an analogy with previous studies [30,31] carried out on the dynamics of laminar flames. In these earlier investigations the scaling involved a characteristic size typically taken equal to the distance between the burner outer lip and the central rod and the laminar burning velocity:

$$\omega^* = \frac{2\pi R f}{S_L[1-(S_L/U_b)^2]^{1/2}} \tag{5}$$

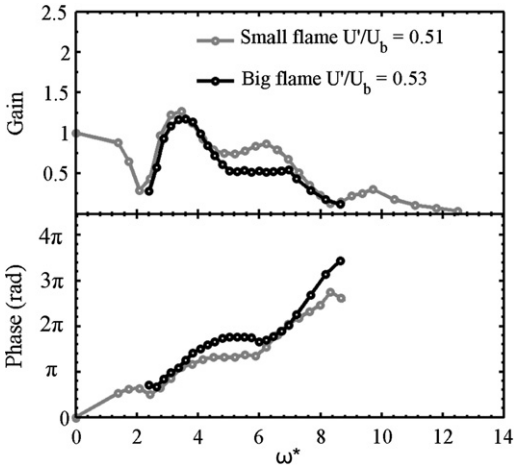

Fig. 7. Nondimensional flame describing functions for the flame B at $U_b = 4.16\ \mathrm{m\,s^{-1}}$ and $U'/U_b = 0.53$ and for flame A at $U_b = 2.67\ \mathrm{m\,s^{-1}}$ and $U'/U_b = 0.51$.

where R is the characteristic dimension of the burner and S_L designates the laminar burning velocity. The cosine of the flame angle also appears in the denominator of this expression. In the present case, it is more adequate to use a turbulent burning velocity in place of S_L.

$$\omega^* = \frac{2\pi R f}{S_T[1-(S_T/U_b)^2]^{1/2}} \tag{6}$$

Here $R = b - a$ is a characteristic dimension of the flame base, where b is the outer diameter of the burner and a is the diameter of the cone, f is the frequency and S_T is the turbulent burning velocity defined by [32] as $S_T = S_L(1 + c(U'_{rms}/S_L)^n)$ where U'_{rms} is the turbulent velocity level with no acoustic modulation. Coefficients $c = 3$ and $n = 0.6$ where extrapolated for methane–air mixtures from measurements made on various fuels. By plotting the gain and phase of two transfer functions corresponding to flames A and B in terms of this reduced angular frequency one obtains Fig. 7. Maximum and minimum values of the gain are located at the same reduced angular frequencies. Around $\omega^* = 2$, a first minimum is reached by the two curves. Then a maximum is reached for $\omega^* = 3.5$ and another minimum is found for $\omega^* = 8.5$. There are some differences in the reduced angular frequency range extending from 4.25 to 7. This difference could be due to the fact that flame B is touching the confinement tube wall while flame A does not. With regard to the evolution of the phase, the two curves collapse but the values obtained for flame B are slightly higher than those found for flame A. The transfer functions composing the flame describing functions also indicate that the flame response is nonlinear (Fig. 6). As the disturbance level is augmented, the gain of the transfer function decreases in the range 0 to 180 Hz or increases in the range extending from 180 to 400 Hz.

4. Unsteady flame dynamics

It is now interesting to analyze the flame dynamics using optical imaging techniques. This could have been achieved by making use of OH PLIF methods [6,7,13] or by directly recording the flame emission with an ICCD camera [8,19]. Observations made, for example, by [7,8,17,25,26] indicate that much of the unsteady flame response is governed by vortex roll-up. A large amplitude of modulation induces flame roll up and the delay of the process is governed by the convective motion. This is well observed in the "V" flame experiments [25,26]. This aspect is however not fully documented in the case of swirling flames. Another observation made in many cases is that the flame anchoring point is moving and that it can be lifted of during part of the cycle [6–8]. It is then natural to examine the unsteady flame dynamics corresponding to the present experiments. This is accomplished by recording the light emission with an ICCD camera. The main objective is to capture the dynamics of the phase conditioned flame front. Six phase-locked images are recorded during an oscillation cycle to define the motion of the flame at the modulation frequency. Each image, separated by a phase angle of 60°, is formed by accumulating one hundred instantaneous images. The resulting data are then compressed by binning adjacent pixels of two by two matrices to decrease the image size and augment the

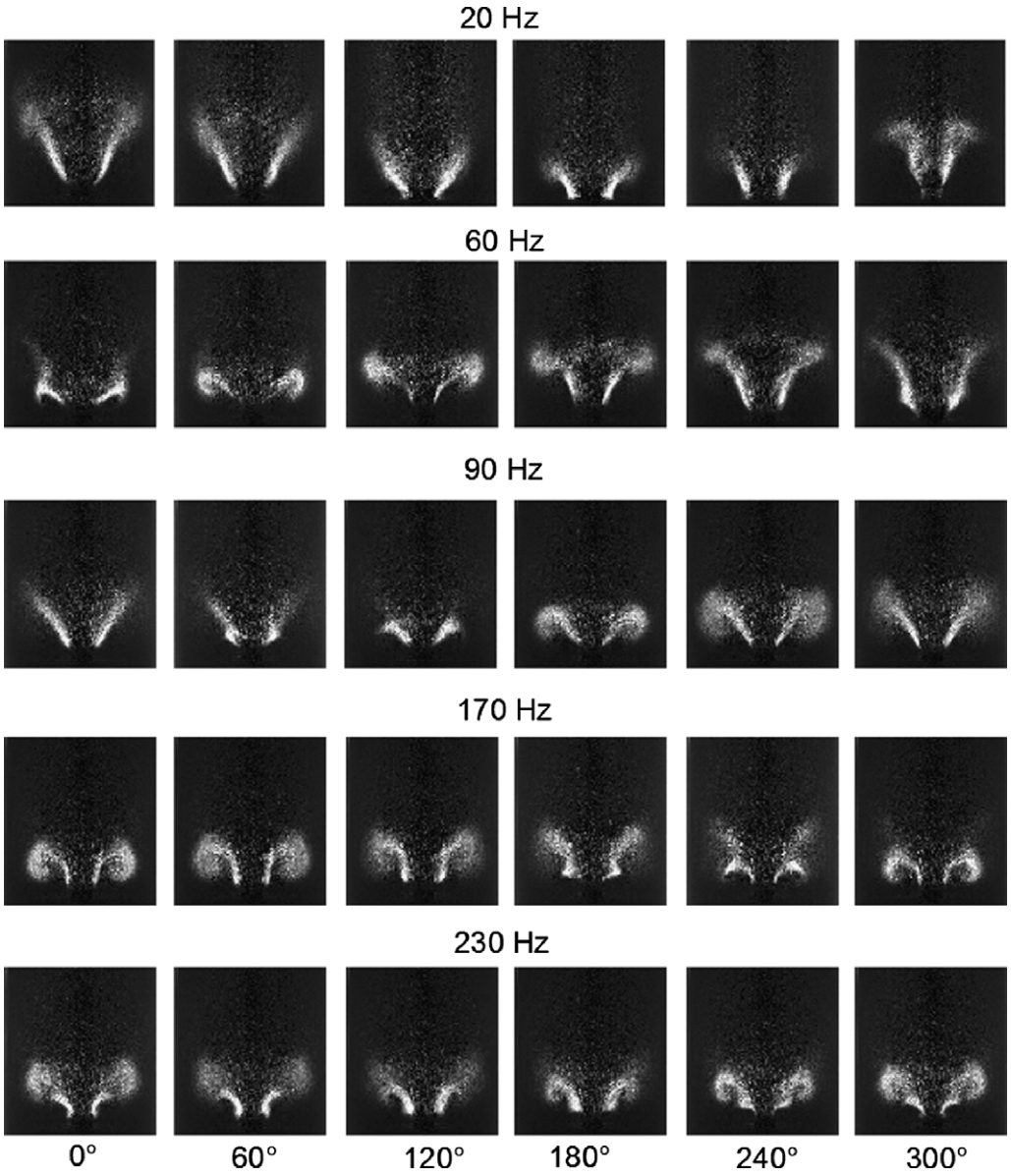

Fig. 8. Flame slice images obtained by phase averaging and Abel transformation of emission images recorded by an ICCD. These images show the evolution of the flame during an oscillation cycle for five frequencies. The mean bulk velocity is $U_b = 2.67\ \mathrm{m\,s^{-1}}$ and the disturbances amplitude is $U'/U_b = 0.51$.

signal to noise ratio. An Abel transform is then applied to each binned image to get the two-dimensional flame slice. This processing is applied to flames A and B described previously. Case A is illustrated by the dynamics observed for the modulation level selected for the transfer function comparison carried out previously (i.e. for $U'/U_b = 0.51$). The flame patterns are shown in Fig. 8. The figure displays the data obtained for five different frequencies corresponding to five characteristic points in the transfer function represented on the left in Fig. 6. These points are located where the gain is maximum, minimum or constant over a range of frequencies. The flame dynamics is described by a full oscillation cycle. All images presented in Fig. 8 are displayed as a function of time expressed in degrees of phase. At 20 Hz, the flame surface is decreasing from 0° to 210° and increasing from 210° to 330°. The gain at 20 Hz (on the left in Fig. 6) according to the transfer function is near one. It is also found that from 90° to 240° flashback takes place with the flame moving slightly backwards into the burner. For the 60 Hz case, between 0° to 90° the flame is

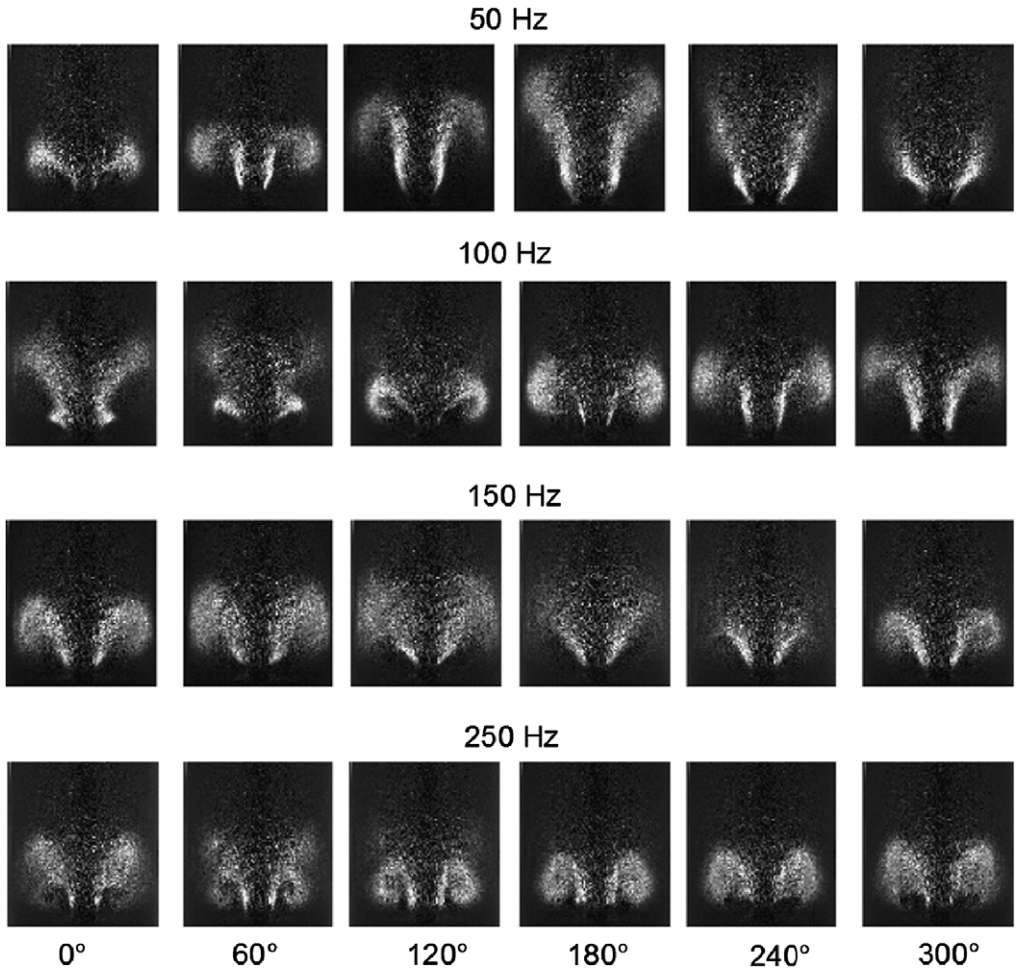

Fig. 9. Flame slice images obtained by phase averaging and Abel transformation of emission images recorded by an ICCD. These images show the evolution of the flame during an oscillation cycle for five frequencies. The mean bulk velocity is $U_b = 4.16\ \mathrm{m\,s^{-1}}$ and the disturbances amplitude is $U'/U_b = 0.53$.

subjected to a convective roll-up motion but the flame surface does not change significantly. From 120° to 210° the convective motion is still present but the flame surface is affected and increases substantially. After 210° and up to 330°, the flame surface is decreasing and the tip of the flame ejects a lump which is rolled-up. It is worth noting that in the 60 Hz case, the gain of the transfer function is quite small (around 0.25, on the left in Fig. 6). At a frequency of 90 Hz, from 0° to 120° the flame surface is decreasing approaching a minimum level at 120°. From 120° to 330°, vortex roll-up acts on the flame and specifically on the flame tips. The gain at 90 Hz is near 1.25. At 170 Hz, from 0° to 120°, a first vortex roll-up occurs without significantly modifying the flame surface. From 150° to 210° emission from the first vortex roll-up has vanished but a second vortex roll-up occurs wrinkling a large amount of flame. From 240° to 330°, the second vortex roll-up is convected smoothly increasing the flame surface. At 170 Hz, the gain of the transfer function is close to 0.75. At 230 Hz, from 0° to 90°, it is observed that the main vortex roll-up occurs at the flame tips but a second wrinkle appears near the nozzle burner. After that, from 120° to 180° the main vortex roll-up progressively disappears while the second roll-up wrinkles the flame base. From 210° to 330°, the second vortex becomes dominant and propagates along the flame. It should be noted that during the cycle, the flame is changing its shape but its surface remains nearly constant. The transfer function gain is close to 0.2.

The dynamics observed for flame B corresponds to a modulation level which nearly coincides with that used for flame A ($U'/U_b = 0.53$). The flame patterns are shown in Fig. 9. The motion observed in these images is quite similar to that described previously subject to the frequency scaling defined in the previous section. For example, the motion

at $f = 150$ Hz for flame B is comparable to that observed at $f = 90$ Hz for flame A with some differences. Similarly the motion at $f = 100$ Hz for flame B is very close to that recorded at $f = 60$ Hz for flame A. For this comparison, it is necessary to shift the phase angles so that the initial flame pattern nearly coincides. Results reported in this section can be used to interpret the describing function measurements and they constitute a database for future comparisons with unsteady simulations.

5. Conclusion

The dynamics of swirled premixed flames is considered in this article. The mean flow is first characterized and the swirl number is deduced from measured velocity profiles. The flame response is then determined for two values of the mass flow rate by considering different levels of modulation. This yields families of transfer functions which constitute a flame describing function (FDF). The FDF depends on the frequency and amplitude of the incoming perturbation and can be used in nonlinear analysis of instabilities driven by this type of flame. Data indicate that the transfer function gain depends on the input level most notably in frequency ranges where this gain reaches its maximum. The phase is less dependent on the input level and features a quasi linear behavior with respect to frequency indicating that the flame responds with a delay to the incoming perturbations. It is found that transfer functions corresponding to different mass flow rates but to a fixed value of the modulation amplitude can be collapsed by making use of a reduced frequency. Systematic observations of the flame motion based on emission images which are phase averaged and Abel transformed indicate that the flame response is governed by the unsteady evolution of the flame shape and surface area. The nonlinear response is mainly associated to the unsteady lift-off affecting the anchor point and to the flame roll-up by vortices formed at the injector exhaust section.

Acknowledgements

This study is part of the MICCA project supported by the Agence nationale de la recherche, contract number ANR-08-BLAN-0027-01.

References

[1] S. Candel, Combustion dynamics and control: Progress and challenges, Proceedings of the Combustion Institute 29 (2002) 1–28.
[2] T. Lieuwen, K. McManus, Introduction: combustion dynamics in lean-premixed prevaporized gas turbines, Journal of Propulsion and Power 19 (2003) 721.
[3] N. Syred, A review of oscillation mechanisms and the role of the precessing vortex core (PVC) in swirl combustion systems, Progress in Energy and Combustion Science 32 (2006) 93–161.
[4] D.G. Lilley, Swirl flows in combustion: a review, AIAA Journal 15 (8) (1977) 1065–1078.
[5] A.K. Gupta, D.G. Lilley, N. Syred, Swirl Flows, Abaqus Press, 1984.
[6] S.K. Thumuluru, H.H. Ma, T. Lieuwen, Measurements of the flame response to harmonic excitation in a swirl combustor, AIAA Paper 2007-0845, Reno, US, 2007.
[7] B.D. Bellows, M.K. Bobba, A. Forte, J.M. Seitzman, T. Lieuwen, Flame transfer function saturation mechanisms in a swirl-stabilized combustor, Proceedings of the Combustion Institute 31 (2007) 3181–3188.
[8] B.D. Bellows, M.K. Bobba, J.M. Seitzman, T. Lieuwen, Nonlinear flame transfer function characteristics in a swirl-stabilized combustor, ASME Paper GT2006-91119, in: ASME Turbo Expo 2006, vol. 129, Barcelona, Spain, 2007, pp. 954–961.
[9] A.X. Sengissen, J.F. Van Kampen, R.A. Huls, G.G.M. Stoffels, J.B.W. Kok, T.J. Poinsot, LES and experimental studies of cold and reacting flow in a swirled partially premixed burner with and without fuel modulation, Combustion and Flame 150 (2007) 40–53.
[10] C.O. Paschereit, E.J. Gutmark, Enhanced performance of a gas-turbine combustor using miniature vortex generators, Proceedings of the Combustion Institute 29 (2003) 123–129.
[11] F.E.C. Culick, Dynamics of combustion systems: fundamentals, acoustics and control, in: RTO AVT Course on "Active control of engine dynamics", Von Karman Institute Rhode Saint Genese, Belgium, 2001.
[12] J.C. Broda, S. Seo, R.J. Santoro, G. Shirhattikar, V. Yang, An experimental study of combustion dynamics of a premixed swirl injector, Proceedings of the Combustion Institute 27 (1998) 1849–1856.
[13] S.Y. Lee, S. Seo, J.C. Broda, S. Pal, R.J. Santoro, An experimental estimation of mean rate and flame structure during combustion instability in a lean premixed gas turbine combustor, Proceedings of the Combustion Institute 28 (2000) 775–782.
[14] C.J. Lawn, Thermo-acoustic frequency selection by swirled premixed flames, Proceedings of the Combustion Institute 28 (2000) 823–830.
[15] D. Fritsche, M. Füri, K. Boulouchos, An experimental investigation of thermoacoustic instabilities in a premixed swirl-stabilized flame, Combustion and Flame 151 (2007) 29–36.
[16] W. Meier, P. Weigand, X.R. Duan, R. Giezendanner-Thoben, Detailed characterization of the dynamics of thermoacoustic pulsations in a lean premixed swirl flame, Combustion and Flame 150 (2007) 2–26.

[17] D.M. Kang, F.E.C. Culick, A. Ratner, Combustion dynamics of a low-swirl combustor, Combustion and Flame 151 (2007) 412–425.
[18] P. Weigand, W. Meier, X.R. Duan, W. Stricker, M. Aigner, Investigations of swirl flames in a gas turbine model combustor I. Flow field, structures, temperature, and species distributions, Combustion and Flame 144 (2006) 205–224.
[19] C. Külsheimer, H. Büchner, Combustion dynamics of turbulent swirling flames, Combustion and Flame 131 (2002) 70–84.
[20] H.C. Mongia, Perspective of combustion modeling for gas turbine combustors, AIAA Paper 2004-0156, 2004, pp. 1–33.
[21] S. Roux, G. Lartigue, T. Poinsot, U. Meier, C. Berat, Studies of mean and unsteady flow in a swirled combustor using experiments, acoustic analysis, and large eddy simulations, Combustion and Flame 141 (2005) 40–54.
[22] F.F. Grinstein, C. Fureby, LES studies of the flow in a swirl gas combustor, Proceedings of the Combustion Institute 30 (2005) 1791–1798.
[23] Y. Huang, V. Yang, Effect of swirl on combustion dynamics in a lean-premixed swirl-stabilized combustor, Proceedings of the Combustion Institute 30 (2005) 1775–1782.
[24] M. Freitag, J. Janicka, Investigation of a strongly swirled unconfined premixed flame using LES, Proceedings of the Combustion Institute 31 (2007) 1477–1485.
[25] D. Durox, T. Schuller, S. Candel, Combustion dynamics of inverted conical flames, Proceedings of the Combustion Institute 30 (2005) 1717–1724.
[26] R. Balachandran, B.O. Ayoola, C.F. Kaminski, A.P. Dowling, E. Mastorakos, Experimental investigation of the nonlinear response of turbulent premixed flames to imposed inlet velocity oscillations, Combustion and Flame 143 (2005) 37–55.
[27] D. Durox, S. Ducruix, F. Lacas, Flow seeding with an air nebulizer, Experiments in Fluids 27 (1999) 408–413.
[28] T. Schuller, D. Durox, S. Candel, Self-induced combustion oscillations of laminar premixed flames stabilized on annular burners, Combustion and Flame 135 (2003) 525–537.
[29] N. Noiray, D. Durox, T. Schuller, S. Candel, A unified framework for nonlinear combustion instability analysis based on the flame describing function, Journal of Fluid Mechanics 615 (2008) 139–167.
[30] T. Schuller, D. Durox, S. Candel, A unified model for the prediction of laminar flame transfer functions comparisons between conical and V-flame dynamics, Combustion and Flame 134 (2003) 21–34.
[31] S.H. Preetham, T. Lieuwen, Nonlinear flame-flow transfer function calculations: flow disturbance celerity effects, in: 40th AIAA/ASME/SAE/ASEE, Joint Propulsion Conference & Exhibit, Fort Lauderdale, Florida, 2004.
[32] N. Peters, Turbulent Combustion, Cambridge University Press, Cambridge, 2000.